Diamagnetism in the normal state of $YBa_2Cu_3O_7$

R. E. Walstedt, R. F. Bell, L. F. Schneemeyer, J. V. Waszczak, and G. P. Espinosa
AT&T Bell Laboratories, Murray Hill, New Jersey 07974
(Received 25 January 1991; revised manuscript received 8 July 1991)

Precise ^{63}Cu NMR shift results are reported for both copper sites in oriented powder samples of $YBa_2Cu_3O_{7.0}$, in which the weak normal-state temperature dependences are resolved. Magnetic-susceptibility data are also given, which, in spite of the presence of small Curie-like terms, are shown to have the same intrinsic temperature dependence as data recently presented by Lee, Klemm, and Johnston. A combined analysis of shift and susceptibility data is described, in which we obtain (1) a partition of the spin paramagnetism between the chain and plane sites, (2) a full description of the susceptibility and hyperfine interaction tensors based only on static measurements, and (3) extracted values for temperature-dependent diamagnetism under field orientation both along the c axis and in the ab plane. The c-axis diamagnetism is large and decays with temperature in a fashion consistent with the asymptotic T^{-1} behavior predicted in recent theories. In the ab plane, the diamagnetism sets on at $T\sim 125$ K in what appears to be a dimensional crossover from purely two-dimensional behavior at high temperatures. The analysis also suggests that the actual degree of bulk susceptibility anisotropy is slightly higher than experimentally reported values. The hyperfine parameters are not markedly changed from those given earlier by Mila and Rice.

I. INTRODUCTION

In the high-T_c superconductors a number of bulk properties are found to exhibit unexpected temperature dependences in the normal state.[1] Moreover, fluctuation effects in the vicinity of T_c have been found to be large and to extend upward in temperature over a surprisingly large range.[2–5] Such a result for the superconducting fluctuation diamagnetism (SFD) has recently been obtained by Lee, Klemm, and Johnston[3] (LKJ), using high-quality magnetically oriented powder samples. In this study, the authors confined their analysis to the anisotropy of the measured susceptibility $\chi_\nu^{\rm expt}(T)$ ($\nu=ab$ or c), on the assumption that any background temperature dependences present in the data in addition to the SFD would be very nearly isotropic and thus cancel. The resulting curve was shown to agree with a Lawrence-Doniach[6] model calculation of the SFD using suitably chosen parameter values. Similar data for the anisotropy of $\chi_\nu^{\rm expt}$ have also been reported by Miljak *et al.*[7] without a detailed theoretical interpretation.

In this paper we present a similar study using a somewhat different approach. In addition to bulk susceptibility data, NMR shifts measured at the Cu(1) and Cu(2) sites in Y-Ba-Cu-O are used to calibrate the temperature dependence of the spin paramagnetism in this material, with the consequence that the full SFD effects [$\chi_\nu^{\rm SFD}(T)$] for fields along both the c axis ($\nu=c$) and in the ab plane ($\nu=ab$) can be examined. As in LKJ, a large c-axis diamagnetic response is found near T_c. However, our results differ considerably from theirs in detail, in that (a) we find the c-axis diamagnetism to decay rather more slowly with temperature and (b) we see a distinct onset of ab-plane diamagnetism below $T\sim 125$ K as well. The disparity between our result for $\chi_c^{\rm SFD}(T)$ and that of LKJ can be traced to their assumption of isotropic spin paramagnetism, as contrasted with our employment of the g-factor anisotropy dictated by the Cu^{2+} ionic model employed by Mila and Rice.[8] This model is invoked here in detail to analyze the magnetic and hyperfine parameters of the system. The g-factor effects are discussed at length in the text. The onset of $\chi_{ab}^{\rm SFD}(T)$ just above T_c appears to represent a dimensional crossover in the diamagnetism. Since LKJ analyzed only the anisotropy of the diamagnetism, they presented no separate result for the in-plane response. In Sec. III we compare our data with results from a class of gauge-fluctuation theories which have been developed to describe the normal-state properties of the high-T_c systems.[9,10]

Precise measurements of the weakly temperature-dependent Cu(1)- and Cu(2)-site shifts in the normal state also makes possible an analysis of the spin paramagnetism into separate contributions from those sites. In the Mila-Rice (MR) treatment of hyperfine phenomena in this material[8] it was assumed, for want of more detailed information, that the Cu(1)- and Cu(2)-site spin susceptibilities are equal and isotropic. Using data given in this paper along with low-temperature NMR shift results from the literature,[11] we are able to relax these assumptions and obtain the susceptibility and hyperfine tensors at both copper sites with their full anisotropy.

The fundamental relation for interpreting the intrinsic susceptibility tensor in this system is

$$\chi_\nu^{\rm expt}(T)=\chi_\nu^{s}(T)+\chi_\nu^{\rm orb}+\chi^{\rm dia}+\chi_\nu^{\rm SFD}(T)\ , \tag{1}$$

where $\nu=ab$ or c. The first two terms represent spin and (Van Vleck) orbital paramagnetism, respectively. $\chi^{\rm dia}$ is the core diamagnetism, and $\chi_\nu^{\rm SFD}(T)$ denotes the normal-state SFD term. Any Landau diamagnetism present will

be included in $\chi_\nu^{\rm SFD}(T)$, the zero of which is experimentally uncertain. In order to analyze $\chi_\nu^s(T)$, we use Eq (1) to isolate this quantity by deriving values for the remaining terms from other considerations. $\chi^{\rm dia}$ can be estimated from tabulated data[12] within narrow limits. We use measurements of the temperature-independent orbital shifts $K_{1,2\nu}^{\rm orb}$ at the Cu(1,2) sites and the relations $\chi_\nu^{\rm orb}=\chi_{1\nu}^{\rm orb}+2\chi_{2\nu}^{\rm orb}$ (Ref. 13) and

$$K_{1,2\nu}^{\rm orb}=\alpha_{\rm orb}\chi_{1,2\nu}^{\rm orb} \tag{2}$$

to evaluate $\chi_\nu^{\rm orb}$, where $\alpha_{\rm orb}=22.41\langle r^{-3}\rangle$.[14] The SFD term is undetermined at the outset, but is presumably negligible above some onset temperature. Above that point we may take $\chi_\nu^s(T)\approx\chi_\nu^{\rm expt}(T)-\chi^{\rm dia}-\chi_\nu^{\rm orb}$. Having thus extracted $\chi_\nu^s(T)$, we can use the companion relations to Eq. (2), $\chi_\nu^s=\chi_{1\nu}^s+2\chi_{2\nu}^s$ and

$$K_{1,2\nu}^s=\alpha_{1,2\nu}^s\chi_{1,2\nu}^s\ , \tag{3}$$

for the spin-paramagnetic shifts $K_{1,2\nu}^s$ to obtain the relation

$$K_{1\nu}^s/\chi_\nu^s=\alpha_{1\nu}^s-2(\alpha_{1\nu}^s/\alpha_{2\nu}^s)(K_{2\nu}^s/\chi_\nu^s)\ . \tag{4}$$

Equation (4) is a linear relation between experimentally derived quantities ($K_{1,2\nu}^s/\chi_\nu^s$), from which we can extract the shift coefficients $\alpha_{1,2\nu}^s$. The partition of χ_ν^s follows then from Eq. (3). These equations serve another important function in identifying, through the implied linear behavior, the range of temperatures over which the $\chi_\nu^{\rm SFD}$ are negligible. Below this range Eq. (4) breaks down, at which point we may use the coefficients $\alpha_{1,2\nu}^s$ with shift data to determine χ_ν^s and thus $\chi_\nu^{\rm SFD}(T)$ through Eq. (1).

In principle, the foregoing scheme only requires reasonable values for $\alpha_{\rm orb}$ and $\chi^{\rm dia}$ to be carried through. In practice it is only possible to measure $K_{1c}^s(T)$ and $K_{2ab}^s(T)$ with enough accuracy to be useful in Eq. (3) and (4), the other components (K_{1ab}^s and K_{2c}^s) being inaccessible for technical reasons. In order to proceed with the analysis one must then also try to deduce the anisotropy of $\chi_{1,2\nu}^s$. In MR these anisotropies were presumed to be small and were ignored. There is, however, electronic g-factor anisotropy in the spin Hamiltonian,[15] owing to spin-orbit coupling matrix elements to the excited states of the Cu^{2+} ($3d^1$) ion. This is a 10–15% effect for the Cu(2) ions.[16] For a d-band susceptibility, where $\chi_\nu^s\propto g_\nu^2$, the anisotropy will be twice as great. Because of stronger mixing of the d_Γ orbitals in the Cu(1) ground state,[8] the anisotropy of $\chi_{1\nu}^s$ is expected to be smaller, and opposite in sign to that of $\chi_{2\nu}^s$. We incorporate these ideas into our analysis in Sec. III, leading to a determination of all susceptibility and hyperfine parameters.

The experimental data for normal-state susceptibility and ^{63}Cu NMR shifts will be presented in Sec. II. The analysis of SFD effects and determination of all relevant parameters are presented in Sec. III. The results and their implications for the behavior of this material are discussed in Sec IV.

II. EXPERIMENTAL RESULTS

A. Sample preparation

High-quality ceramic $YBa_2Cu_3O_{7.0}$ was synthesized using the solid-state reaction method[17] in a procedure which has given uniform results over may repetitions. Following calcination, the ~ 0.7 cm^3 pellet was ground and refired twice at $T\sim 950$° C, then annealed in flowing O_2 for 12 h at $T\sim 450$ °C. X-ray powder photographs showed no indication of a second phase. Susceptibility measurements showed the onset of superconducting diamagnetism at $T\sim 92$ K.

The pellet was broken into several pieces and a solid piece weighing 0.35 g was selected for the experiments. An initial susceptibility was run (see Sec. II B), showing relatively little of the spurious Curie term which occurs even in very good specimens of this compound. The fragment was finely ground in an agate mortar and subsequently annealed in flowing O_2 at $T\sim 450$ °C overnight to ensure full oxygenation. For magnetic orientation the annealed powder was mixed with a similar volume of clear epoxy in a teflon sample container, and left to cure in the NMR probe in a field of 7.5 T. The sample was not subsequently moved until the first set of NMR measurements reported in Sec. II C was completed.

B. Susceptibilities

Susceptibilities were measured with an electrobalance in variable field up to $B\sim 1.5$ T. The effect of small ferromagnetic inclusions was corrected for by extrapolating plots of M/H vs H^{-1} to $H^{-1}\rightarrow 0$, where M is the measured magnetic moment. Such corrections were typically of order 15%. The background susceptibilities of sample holders and, in the case of the powdered sample, of the epoxy were measured in separate runs and subtracted from the experimental data in proportion to their relative masses in the composite samples. The resulting data are shown in Fig. 1, where the original solid ceramic sample gave curve (a) and the oriented powder sample yielded curves (b) and (c) for field orientations perpendicular and parallel to the c axis, respectively. Curves (d) and (e) are facsimile representations of data from LKJ corresponding to the conditions of curves (b) and (c), respectively. The ceramic (a) shows only slight evidence of a Curie term, whereas there is clearly increased evidence of such terms in the oriented and epoxied samples (b) and (c). We note that the increased Curie effect we observe is not as extreme as the effects reported by Lee and Johnston[18] under nominally similar conditions.

The LKJ data are claimed to be free of the Curie background effect. For our analysis we employ their data on this basis and consider possible effects of a residual Curie contribution in Sec. IV. As such, then, the LKJ data form a useful standard with which to compare our results and determine the nature of the spurious background effects. A key assumption in our procedure is that the intrinsic susceptibilities of the two samples are the same apart from an experimental scale factor and effects having to do with their respective degrees of particle orienta-

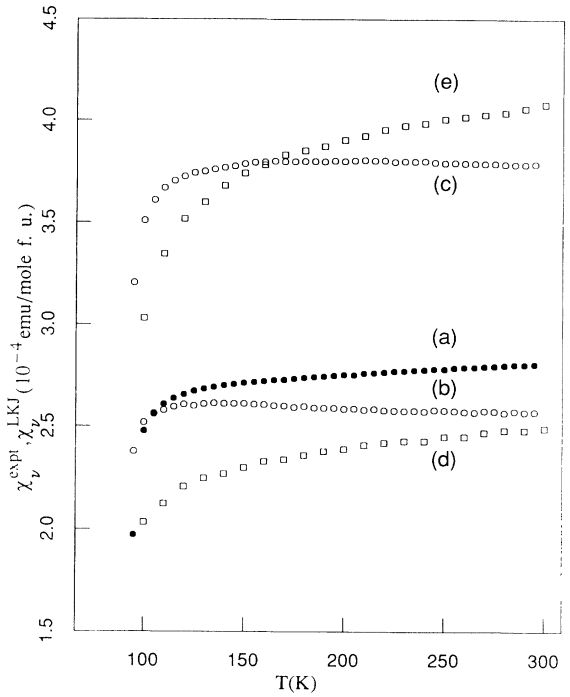

FIG. 1. Measured susceptibilities (a) χ_{pow}^{expt}, (b) χ_{ab}^{expt}, and (c) χ_c^{expt} are plotted vs temperature T. Shown for comparison are facsimile representations of (d) χ_{ab}^{LKJ} and (e) χ_c^{LKJ}.

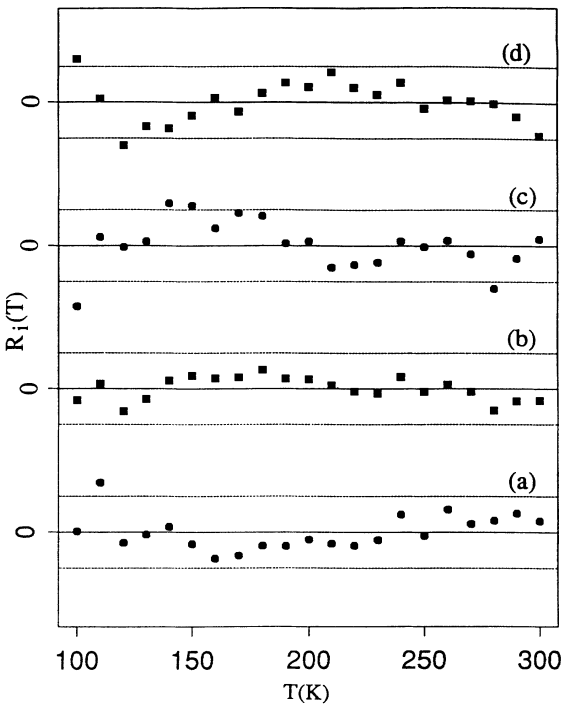

FIG. 2. The residuals $R_i(T)$ from least-squares fits to Eq. (5) for the four cases listed in Table I are plotted as a function of temperature, where $R_i(T)$ is defined in the text. The dashed lines indicate deviations of ±0.5%.

tion, the latter effect being easily adjusted for. There are good reasons for this assumption to be valid for high quality, well-oxygenated samples of Y-Ba-Cu-O. NMR shifts and relaxation times reported for ^{63}Cu in this material by many laboratories are found to agree within experimental error, despite the presence of a variable amount of the Curie-like background susceptibility. To an excellent approximation, the shifts depend only on the intrinsic paramagnetism. The results of Alloul, Ohno, and Mendels[19] on ^{89}Y shifts in a series of oxygen-deficient Y-Ba-Cu-O samples show that oxygen content is the main variable which alters the intrinsic susceptibility. We have carefully monitored the sample oxygenation, as presumably have LKJ (see below).

We have compared our data with that of LKJ quantitatively by performing least-squares fits to the form

$$\chi_i^{expt}(T)=S\chi_i^{LKJ}(T)+C/T\ , \tag{5}$$

where $\chi_i^{expt}(T)$ and $\chi_i^{LKJ}(T)$ represent suitable combinations of values measured by us and by LKJ, respectively. The combinations studied are shown in Table I along with the fitting parameters. For example, we have fit our original ceramic data $\chi_{cer}^{expt}(T)$ and the powder average $[\chi_c^{expt}(T)+2\chi_{ab}^{expt}(T)]/3$ (both as χ_i^{expt}) to the powder average

$$\chi_i^{LKJ}(T)=[\chi_c^{LKJ}(T)+2\chi_{ab}^{LKJ}(T)]/3$$

of the LKJ values from Fig. 1. The residuals

$$R_i(T)=[\chi_i^{expt}(T)-S\chi_i^{LKJ}(T)-C/T]/\chi_i^{expt}(T)$$

from these two fits are displayed in Figs. 2(a) and 2(b), respectively, showing the rms errors to be less than 0.5%.

To examine the uniqueness of fits to Eq. (5), the fits represented in Figs. 2(a) and 2(b) have been repeated with the more general form

$$\chi_i^{expt}(T)=S\chi_i^{LKJ}(T)+C/(T+\Theta)+D\ ,$$

allowing a Curie-Weiss constant Θ and a constant term

TABLE I. Least-squares fitting parameters C and S from Eq. (5) for various pairs of susceptibilities $\{\chi_i^{expt},\chi_i^{LKJ}\}$. Errors given are two standard deviations. The Curie constants C are given in units of 10^{-3} Kemu/mole f.u. For the fits labeled 2*c* and 2*d*, the LKJ data (Fig. 1) were adjusted to match the room-temperature anisotropy $A_{expt}=1.49$ of the data reported here (after corrections, Fig. 3), using Eqs. (A6).

Figure	χ_1^{expt}	χ_i^{LKJ}	S	C
2a	χ_{cer}^{expt}	$(2\chi_{ab}^{LKJ}+\chi_c^{LKJ})/3$	0.886±0.004	5.79±0.30
2b	$(2\chi_{ab}^{expt}+\chi_c^{expt})/3$	$(2\chi_{ab}^{LKJ}+\chi_c^{LKJ})/3$	0.911±0.003	10.60±0.20
2c	χ_{ab}^{expt}	χ_{ab}^{LKJ}	0.912±0.005	9.44±0.40
2d	χ_c^{expt}	χ_c^{LKJ}	0.909±0.005	12.93±0.50

D, in addition to S and C as variables. Both cases yielded Θ of order 1 K and D of less than 1% of $\chi_i^{\text{expt}}(T)$. The residuals were virtually unchanged from the values in Fig. 2. Thus, Θ and D are driven by noise alone and represent no real physical effect. We therefore conclude that our ceramic and powder average data are given very precisely by a scale factor times the corresponding LKJ average plus a Curie term. Whether the spurious term is taken to be Curielike or Curie-Weiss like is immaterial.

The foregoing results support our assumption of identical intrinsic susceptibilities and establish, further, that we can obtain a close approximation to intrinsic behavior by subtracting a correction term of Curie form. While it is difficult to prove uniqueness in using Eq. (5), the basic soundness of this approach is supported by three observations. First, the residuals [Figs. 2(a) and 2(b)] consist almost entirely of random noise. Second, the Curie form determined is consistent with the simple hypothesis of stray localized moments in the Y-Ba-Cu-O lattice as the source of this term. And, finally, the scale factor S (Table I) determined in the three fits of our oriented powder to the LKJ data lie within a range of less than 0.5%, the ceramic value lying $\sim 2\%$ below that.

In Figs. 2(c) and 2(d) we show the residuals from fitting our c-axis and ab-plane-oriented powder data to $\chi_c^{\text{LKJ}}(T)$ and $\chi_{ab}^{\text{LKJ}}(T)$, respectively. An important step in this process is to adjust the LKJ reference data to have the same room-temperature anisotropy as ours. Thus,

$$A_{\text{LKJ}} = \chi_c^{\text{LKJ}}(300\text{ K})/\chi_{ab}^{\text{LKJ}}(300\text{ K}) = 1.61$$

(Fig. 1) must be changed by linear transformation to $A_{\text{expt}} \sim 1.49$, the value we find after corrections. The required transformations are derived in the Appendix. In this way, the $\chi_v^{\text{tot}}(T)$ for the two samples is compared as though they possessed the same degree of particle orientation. The residuals for these two fits show a small apparent difference ($<1\%$) in intrinsic behavior just above T_c, which might arise from a minor disparity in oxygenation or in T_c, itself. This does not materially affect the analysis and results given below.

An interesting surprise which arises in fitting the oriented powder data is the appearance of an anisotropic Curie constant (Table I). This effect is resolved well beyond the errors. The validity of the result is underscored by the precise match in scale factors S for the two fits. No significant change in the anisotropy of C or improvement of the fits is effected by adding the parameters Θ and D as described above. The apparent meaning of the anisotropy, discussed further in Sec. IV, is that the Curie term arises from local moments in disordered regions of the Y-Ba-Cu-O lattice. We have proceeded to correct the data in Fig. 1 using the Curie constants in Table I, the results being shown in Fig. 3. It is important to note that our resulting susceptibilities are equivalent to those of LKJ to within the experimental scatter.

The scale factors S in Table I show that our susceptibility values are smaller than those of LKJ by $\sim 10\%$. Our room-temperature powder average magnitude is, in units of 10^{-4} emu/mole f.u., 2.74 in comparison with 2.7 from previous work[20] and ~ 2.8 from the literature.[21,22] The corresponding LKJ value is 3.0. We shall adopt our measured values for subsequent analysis. On the other hand, for anisotropy $A\,(=\chi_c/\chi_{ab})$ the values at room temperature are $A_{\text{expt}} = 1.49$ (this work) as compared with $A_{\text{LKJ}} = 1.61$ and $A = 1.36$ from Ref. 22. Barring technical errors, the largest (LKJ) result is probably the most nearly correct. The true value may actually be larger than A_{LKJ}. In the analysis of Sec. III we shall consider A to be a variable parameter, constructing curves for $\chi_v^{\text{tot}}(T)$ from our corrected data using Eqs. (A6a) and (A6b).

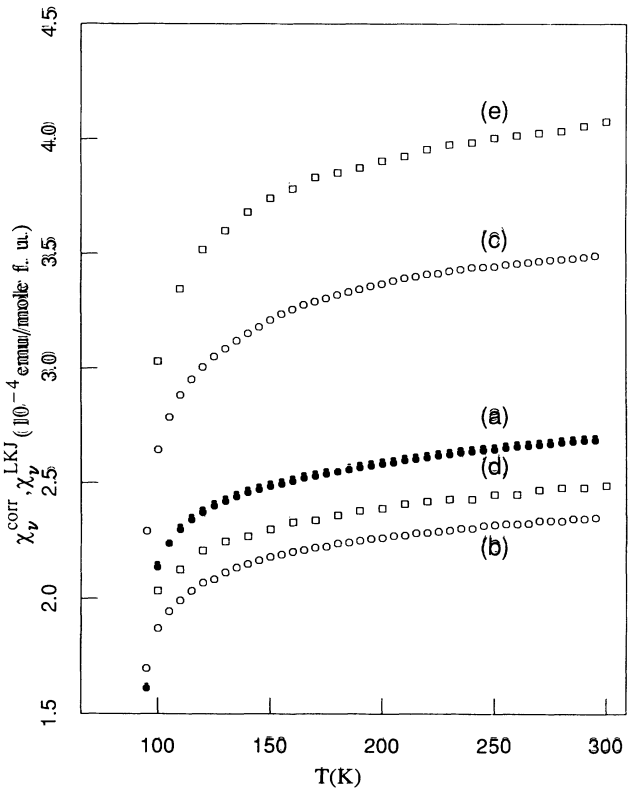

FIG. 3. Curves (a), (b), and (c) show the corresponding susceptibility data plots from Fig. 1 after subtracting the spurious Curie terms determined by fitting Eq. (5) to the appropriate pairings of the measured susceptibilities and those given by LKJ. The facsimile plots of (d) χ_{ab}^{LKJ} and (e) χ_c^{LKJ} are again shown for comparison.

C. ^{63}Cu NMR shift measurements

In order to implement the scheme described in Sec. I, we have performed measurements of the ^{63}Cu NMR shifts K_{1c} and K_{2ab} over the temperature range $95 \le T \le 300$ K with a precision several times greater than previously reported in the literature. As for the other shift components, K_{1a} and K_{1b} are difficult to measure accurately, because the Cu(1) site presents a powder pattern spectrum with the field in the ab plane.[22] On the other hand the shift K_{2c} can be determined very precisely, because the Cu(2)-site NMR line for this orientation is very narrow as shown in Fig. 4. The problem here is that α_{2c}^s is, by accident, very nearly zero. The change in K_{2c}

below T_c,[11] as the spin paramagnetism decays to zero, is itself very difficult to resolve. As expected, then, the change of K_{2c} in the normal state up to room temperature is unmeasurably small. This point is illustrated in Fig. 4, where we display data at $T=100$ and 290 K. There is a slight increase in linewidth on cooling and also a slight change in the *apparent* position of the peak. The solid lines drawn are a model line shape consisting of a Gaussian distribution of angular deviations from exact alignment along the c axis, which gives an asymmetric broadening to higher field from second-order quadrupolar shifts,[23] combined with inhomogeneous broadening which is also Gaussian. The latter broadening is greater at $T=100$ K, giving an apparent shift of position. The shift is actually taken to be the same from both calculated curves. Thus, we can resolve no change in K_{2c} to within 0.002%. The angular distribution for these model curves has a Gaussian width $\sim 1.5°$, showing that the oriented portion of the sample is very well oriented, indeed.

The Cu(2)-site shift K_{2ab} is a much better probe of the planar spin paramagnetism. Data for the variation of K_{2ab} with temperature were taken using line profiles such as that shown in Fig. 5 for $T=100$ K. The NMR line is somewhat broader with the field in the ab plane than with the field along the c axis (Fig. 4). There are several reasons for this. First, the asymmetric quadrupolar broadening is ~ 2.5 times greater near the $\Theta=\pi/2$ singularity than it is at $\Theta\sim 0$.[23] Second, the axial character of the electric field gradient (EFG) tensor is only approximate for the Cu(2) site; small deviations from $\eta=0$ will also broaden this peak. Also, the paramagnetic shift broadening may be increased by a slight in-plane shift anisotropy on account of the orthorhombic symmetry.

The solid curve in Fig. 5 is a functional fit to the central portion of the line profile. The linewidth changes by only $\sim 20\%$ over the range of temperatures studied; thus, we measure the shift from the peak of the fitted curve. In addition to the NMR shift K_{2ab} this line undergoes a second-order quadrupolar shift[23] given quite accurately by $\Delta\nu=\nu_{\rm res}-\nu_L\approx 3\nu_Q^2/16\nu_L$, where ν_Q is the NQR frequency and $\nu_L=\gamma H_0(1+K_{2ab})$. In extracting the shift from these data, it is important to include the temperature dependence of ν_Q. Measurements of ν_Q were carried out using the position of the first-order quadrupolar satellite in high field relative to the $m=\pm\frac{1}{2}$ transition, yielding a temperature dependence in agreement with that derived from NQR.[24] Our final result for K_{2ab} is the curve shown as dots in Fig. 6.

These values for K_{2ab} are in reasonable accord with values from the literature,[11] but show two new features. First, there is a gradual linear increase in K_{2ab} with decreasing temperature, in opposition to the behavior of the susceptibility (Fig. 3). This leads to the surprising conclusion that the temperature variation of χ^s_{ab} is dominated by the chain-site contribution χ^s_{1ab}. The observed increase in K_{2ab} is supported by data on the ^{89}Y shift in Y-Ba-Cu-O,[25] which also increases in magnitude at lower temperatures, at a rate $dK_{^{89}Y}/dT\sim 0.17$ ppm/K. Using

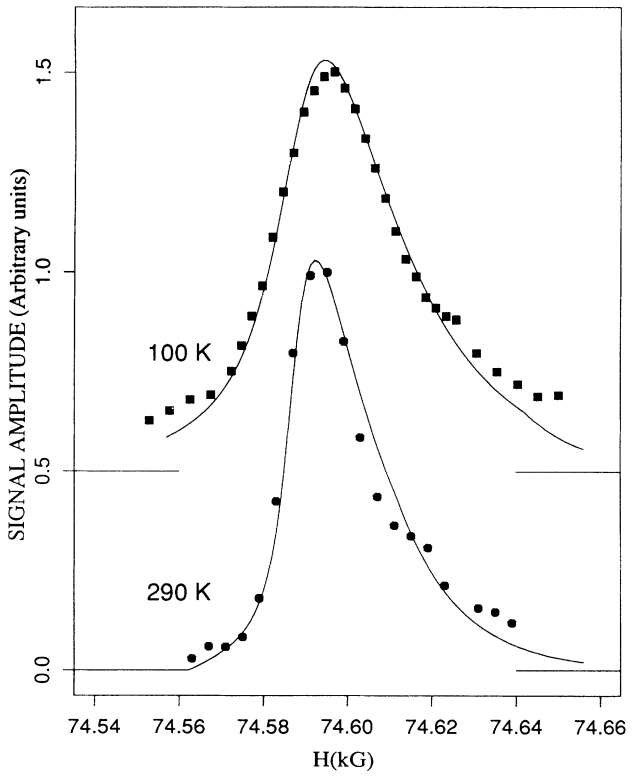

FIG. 4. The ^{63}Cu(2) $m=\pm\frac{1}{2}$NMR line in Y-Ba-Cu-O is shown at a frequency of 85.245 MHz, with the field oriented along the c axis, for temperatures $T=100$ and 290 K. The solid lines are functional fits to the data (see text), showing that there is no measurable change in shift between these temperatures.

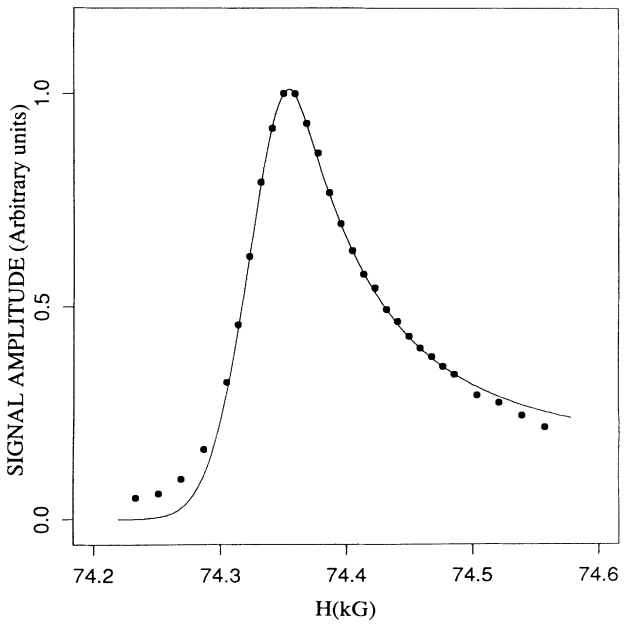

FIG. 5. A typical ^{63}Cu(2) NMR line scan is shown (dots) for field oriented in the ab plane, here at a frequency of 86.55 MHz and a temperature of 100 K. The solid line is a functional fit to the data points near the center of the line. The shift values quoted refer to the peak of the spectrum and are corrected for second-order quadrupolar shift, as discussed in the text.

the ratio of shift coefficients $dK^s_{2ab}/dK_{89} \sim 8.0$ determined for $YBa_2Cu_3O_{6.64}$,[26] one can estimate

$$dK^s_{2ab}/dT \sim (dK^s_{2ab}/dK_{89_Y})(dK_{89_Y}/dT) \sim 1.4 \text{ ppm/K} ,$$

which is about 30% greater than the slope in Fig. 6. Given the uncertainties in such a comparison, we consider the observed correspondence to be satisfactory.

The second feature in the K_{2ab} data is the precursive downturn below 125 K. This is qualitatively similar to behavior reported for K_{89_Y} (Ref. 19) in oxygen-deficient Y-Ba-Cu-O, but more abrupt. A downturn in spin susceptibility above T_c is a characteristic feature of many of the high-T_c compounds.

In contrast with the Cu(2) results, the Cu(1) NMR spectrum reflects more strongly the presence of disorder in the chain layer, exhibiting a marked asymmetric line broadening as the temperature is lowered. This is shown in Fig. 7, where we plot ^{63}Cu(1) NMR spectra for field along the c axis and for temperatures ranging from 95 to 290 K. A similar, though much greater, effect of this sort was reported recently by this laboratory for chain sites in oxygen-deficient Y-Ba-Cu-O.[26] The data in Fig. 7 show a broadening by a factor ~ 3 over the temperature range covered, while the peak position moves gradually to higher fields. The measured susceptibility would reflect the motion of the *center of gravity* (CG) of this line. We have sought to determine the motion of the CG using the solid line fits to these spectra. The fitting function is asymmetric with an exponentially decaying tail on the high-field side. The analysis is complicated somewhat by a broad band of low NMR intensity in the region between the Cu(1) and Cu(2) peaks, the latter lying just off scale to the right. This background intensity results presumably from poorly oriented material in the sample. Our criterion for fitting the Cu(1) peak is to include data on the high-field side up to the point where the amplitude falls to 40% of the peak value. The fits shown are least-squares fitted to data for all fields below that point. The result is that as temperature decreases, a somewhat increasing fraction of the intensity to the right of the peak lies under the fitted curve. Thus, the motion of the CG to higher fields, i.e., lower shift values (shown in Fig. 6 as filled squares), may be slightly exaggerated by the fitting procedure. If so, we prefer to overestimate the temperature slope of the Cu(1) shifts in order not to underestimate the temperature variation of the spin paramagnetism. The motion of the CG shift in Fig. 6 is seen to be

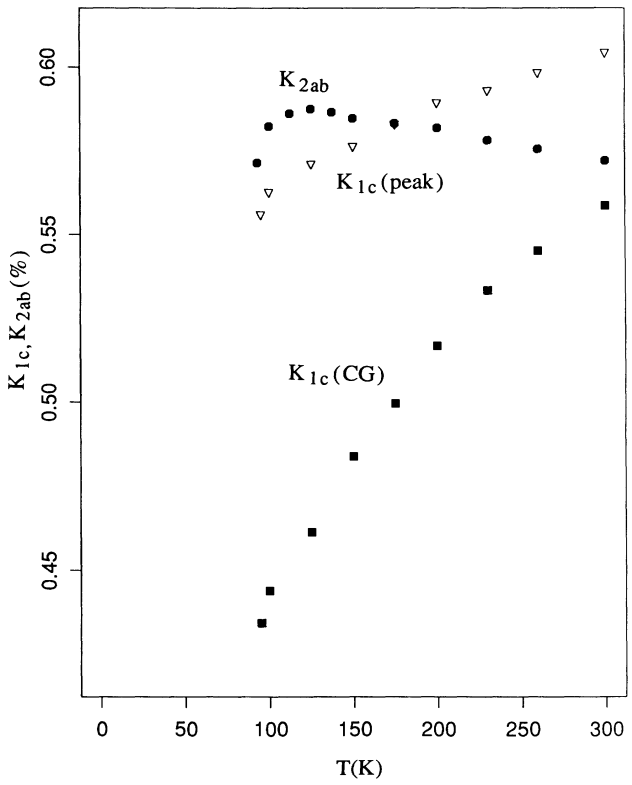

FIG. 6. Normal-state ^{63}Cu NMR shifts for both chain and plane sites in Y-Ba-Cu-O are plotted as a function of temperature. The Cu(2)-site shift K_{2ab} is determined from data such as that shown in Fig. 5 for field oriented in the *ab* plane. The Cu(1)-site shifts are plotted for both the peak position and the center of gravity (CG) of the lines shown in Fig. 7.

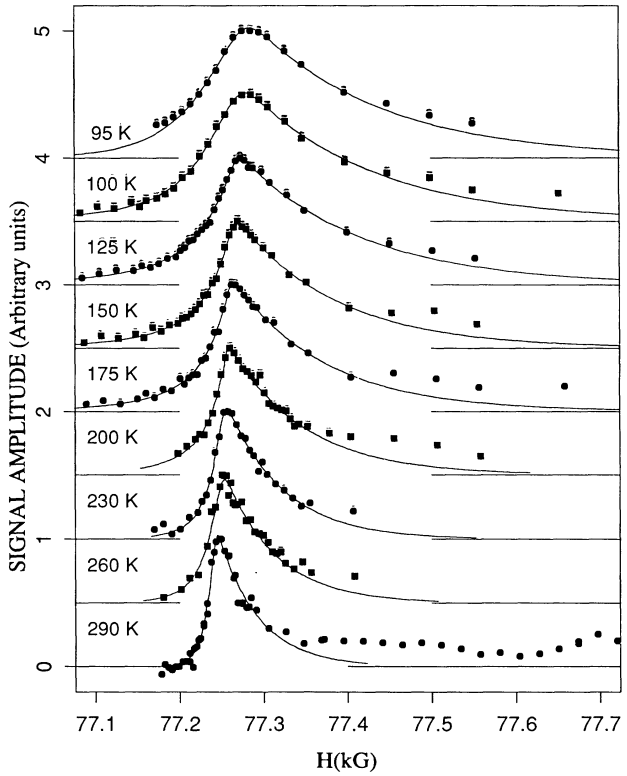

FIG. 7. Cu(1)-site NMR line scans at a frequency of 87.7 MHz with field oriented along the c axis for the range of temperatures indicated. The solid lines are functional fits as described in the text. To the right of the Cu(1) lines is a broad background of NMR intensity which presumably originates from poorly oriented sample material. The trend in the degree of fit in this region is such that the motion of the center of gravity of the Cu(1) line to higher (lower) fields (shifts) may be slightly exaggerated.

much more rapid than that of the Cu(1) peak, shown as open triangles.

III. DATA ANALYSIS

In this section we carry through the analyses outlined in Sec. I, using the shift and susceptibility data presented in Sec. II as well as selected NMR shift results from the literature. As an adjunct to our implementation of Eq. (4) and the related discussion of SFD effects, we also present a scheme to determine the necessary hyperfine parameters and spin polarization anisotropies. Since Eq. (4) is an integral part of that scheme, it is most efficient to describe these developments simultaneously. As noted earlier, we only require values for $\chi^{\rm dia}$ and $\alpha_{\rm orb}$ (i.e., $\langle r^{-3}\rangle$) to extract χ_ν^s from the measured susceptibilities in a region where the SFD is negligible. However, only two of the four shift components, namely K_{2ab} and K_{1c}, are available to use in Eq. (4). To accommodate this restriction we develop estimates of the anisotropies[27]

$$\xi_1=\chi_{1c}^s/\chi_{1ab}^s \quad \text{and} \quad \xi_2=\chi_{2c}^s/\chi_{2ab}^s \ , \tag{6}$$

which we assume to be independent of temperature. Furthermore, since the χ_ν^s in Eq. (4) are not available directly from experiment, we replace them here with the residual susceptibilities

$$\chi_\nu^{\rm res}=\chi_\nu^{\rm tot}-\chi_\nu^{\rm orb}-\chi^{\rm dia}=\chi_\nu^s+\chi_\nu^{\rm SFD} \ ,$$

where components of $\chi_\nu^{\rm tot}$ are derived from the experimental numbers using Eqs. (A6). With these modifications we can rewrite Eq. (4) as

$$K_{1c}^s/\chi_{ab}^{\rm res}=\alpha_{1c}^s\xi_1-2\xi_1(\alpha_{1c}^s/\alpha_{2ab}^s)(K_{2ab}^s/\chi_{ab}^{\rm res}) \tag{7a}$$

and

$$K_{1c}^s/\chi_c^{\rm res}=\alpha_{1c}^s-2\xi_2(\alpha_{1c}^s/\alpha_{2ab}^s)(K_{2ab}^s/\chi_c^{\rm res}) \ , \tag{7b}$$

for $\nu=ab$ and $\nu=c$, respectively, in terms of quantities available from experiment. Where $\chi_\nu^{\rm res}\approx\chi_\nu^s$, i.e., at sufficiently high temperature, plots of $K_{1c}^s/\chi_{ab}^{\rm res}$ against $K_{2ab}^s/\chi_{ab}^{\rm res}$ and $K_{1c}^s/\chi_c^{\rm res}$ against $K_{2ab}^s/\chi_c^{\rm res}$ should yield linear behavior which will enable us to partition χ_{ab}^s and χ_c^s between the sites. Such plots are shown in Fig. 8 based on shift and susceptibility data from Sec. II. The precise conditions for these plots and their implications for SFD effects will be discussed below. For the moment, we focus on the mechanics of using them to establish the various parameter values.

The plot of Eq. (7a) in Fig. 8 shows the linear behavior expected down to $T\sim150$ K, below which a deviation occurs which we identify as the onset of $\chi_{ab}^{\rm SFD}$. The plot for Eq. (7b) does not appear to yield a useful linear region, suggestive of anomalous diamagnetic behavior as we discuss below. The straight line passed through the high-temperature points for Eq. (7a) is a least-squares fit, from which we obtain α_{2ab}^s and, thus, partition χ_{ab}^s into chain and plane-site contributions. To go further we need an estimate of either ξ_1 or ξ_2. We choose to estimate ξ_2 from the bandlike relation $\chi_{2\nu}^s\propto g_{2\nu}^2$, where the

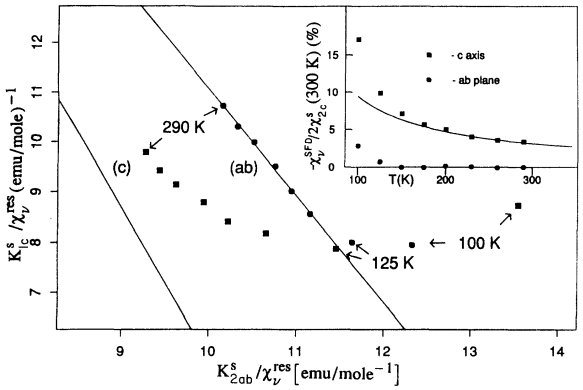

FIG. 8. Plot of $(K_{1c}^s/\chi_\nu^{\rm res})$ vs $(K_{2ab}^s/\chi_\nu^{\rm res})$ for $\nu=ab$ and c, where the residual susceptibility $\chi_\nu^{\rm res}$ is defined in the text. Where SFD effects are negligible, $\chi_\nu^{\rm res}\approx\chi_\nu^s$, and, by Eqs. (7) such plots will yield a straight line. The solid line shown for $\nu=ab$ is a linear regression fit to the data for $T>125$ K. The corresponding line for $\nu=c$ is a plot of Eq. (7b) with the coefficient parameters taken from Table III. The inset shows the temperature-dependent diamagnetism which results from subtracting χ_ν^s values derived from the straight-line fits shown here from experimental values of $\chi_\nu^{\rm res}$. The solid curve passed is a fit to $\chi_c^{\rm SFD}(T)=B/T$ at the high-temperature end.

electronic g factors $g_{2\nu}$ are taken from the ionic model,[15]

$$g_{2ab}=2-2\lambda/\Delta_1 \quad \text{and} \quad g_{2c}=2-8\lambda/\Delta_0 \ . \tag{8}$$

In Eq. (8), λ is the spin-orbit coupling parameter and $\Delta_{0\,(1)}$ the crystal field splitting to the d_{xy} (d_{yz},d_{zx}) excited state. Values for $\Delta_{0\,(1)}$ may be obtained from orbital shift data[11] (and $\langle r^{-3}\rangle$) using ionic model expressions for $\chi_{2\nu}^{\rm orb}$.[8,28] We adopt the estimate $\lambda\approx-0.088$ eV from Cu^{2+} impurity studies.[8,15] These relations lead to a value for $\xi_2=(g_{2c}/g_{2ab})^2$, which in turn gives χ_{2c}^s from χ_{2ab}^s [Eq. (6)]. Finally, we have $\chi_{1c}^s=\chi_c^s-2\chi_{2c}^s$. These steps therefore yield all coefficient parameters in Eqs. (7a) and (7b).

Up to this point, the parameter $\langle r^{-3}\rangle$ has simply been assumed. Further relations from the ionic model allow us to extract this quantity from the shift coefficients $\alpha_{2\nu}^s$ obtained in the previous paragraph [see Eq. (3)], where for K_{2c}^s we adopt the value -0.01% given by Barrett *et al.*[11] The ionic model leads[16] to the relation $\alpha_{2\nu}^s=0.358A_\nu/g_\nu$, where A_ν is the spin hyperfine constant in kilogauss per Bohr magneton. The MR model formulation gives[8]

$$A_\nu=A^{\rm iso}+A_\nu^{\rm s.o.}+D_\nu\langle r^{-3}\rangle \ . \tag{9}$$

In Eq. (9) $A^{\rm iso}=A^{\rm cp}+4B$ is the isotopic hyperfine term consisting of the core-polarization and nearest-neighbor transferred contributions. $A_\nu^{\rm s.o.}$ is a contribution from spin-orbit mixing effects, which is determined by measured values of the orbital shifts[29] combined with our previously mentioned estimate of λ. The final term is the dipolar contribution, where $D_{ab}=17.7$ (a.u.)^3 kG/μ_B and $D_c=-35.5$ (a.u.)^3 kG/μ_B. The unknowns in Eq. (9) are $A^{\rm iso}$ and $\langle r^{-3}\rangle$, which are then determined by values for α_{2ab}^s, α_{2c}^s, and the g factors.

To summarize the arguments of the last few para-

graphs, then, we note that Eqs. (1)–(3), (7a), (8), and (9) along with ancillary relations given with them constitute a coupled set of nonlinear equations for the unknown parameters χ^s_{2ab}, χ^s_{1c}, χ^s_{2ab}, χ^s_{2c}, Δ_0, Δ_1, $\langle r^{-3}\rangle$, and $A^{\rm iso}$. These equations break down into subsets which are not strongly coupled together, and thus are solved easily by iteration. A solution determines the parameters mentioned, and also leads to values for the derived quantities $\chi^{\rm orb}_{1,2\nu}$, $\alpha^s_{1,2\nu}$, $\alpha_{\rm orb}$, $g_{2\nu}$, and $A^{\rm s.o.}_\nu$, i.e., all parameters associated with the static magnetic and hyperfine response.

The data set from which the foregoing parameters are derived consist of the shift and susceptibility data of Sec. II, the four orbital shift components,[11] and $\chi^{\rm dia}$, for which we adopt the empirical estimate $\chi^{\rm dia}\simeq 166\times 10^{-6}$ emu/mole f.u.[12] The specific (room-temperature) values used for these input data are listed in Table II. The only quantity among these about which there remains some uncertainty is the anisotropy A of the measured susceptibility, as we have already noted in Sec. II B. The choice of A will affect all the parameter values to some extent, but is particularly crucial to the value obtained for the local anisotropy ξ_1 [Eq. (6)]. To illustrate this effect we plot in Fig. 9 the derived value for ξ_1 as a function of A. Other input parameters are as given in Table II.[30] As $A=\chi^{\rm tot}_c/\chi^{\rm tot}_{ab}$ is varied, the corresponding values for $\chi^{\rm tot}_\nu$ are extracted from Eq. (A6) using room-temperature input data $\chi^{\rm expt}_\nu$ from Fig. 3.

In Fig. 9 we see that the LKJ value $A_{\rm LKJ}=1.61$ gives $\xi_1\sim 0.7$. While there are no hard data to rule this out, such a value is, in our view, unreasonably small. We argue this point in terms of the ionic model, where the ground-state electronic g factors for the Cu(1) site determine ξ_1 through $\chi^s_{1\nu}\propto g^2_{1\nu}$. The $g_{1\nu}$ depend on the composition of the ground state. Here we refer to the discussion given by MR, who estimate the Fermi-surface Cu(1) orbital composition to be 75% $d_{x^2-y^2}$ and 25% $d_{3z^2-r^2}$. They note that this admixture is consistent with the spin hyperfine constant and the nearly isotropic T_1 process.[31] We add here that the diminished orbital shift anisotropy for Cu(1) is also suggestive of a mixed ground state. For Cu(2) one has[11] $\chi^{\rm orb}_c/\chi^{\rm orb}_{ab}=4.57$. The Cu(1) site has an approximate fourfold axis in the a direction, with $\chi^{\rm orb}_b$ and $\chi^{\rm orb}_c$ differing by $<10\%$.[11] The corresponding shift anisotropy for Cu(1) is $2\chi^{\rm orb}_a/(\chi^{\rm orb}_b+\chi^{\rm orb}_c)=4.15$. This diminished ratio is suggestive of a $\sim 20\%$ admixture of $d_{3z^2-r^2}$, which would make the same contribution to $\chi^{\rm orb}_{b,c}$, but no contribution to $\chi^{\rm orb}_a$.

The g factors would be even more strongly affected, since the $d_{3z^2-r^2}$ ground orbital has an *equal and opposite g-factor anisotropy* to that of Eq. (8).[15] By the arguments of the preceding paragraph one has $\xi_1\simeq 2g^2_{1c}/(g^2_{1a}+g^2_{1b})$.

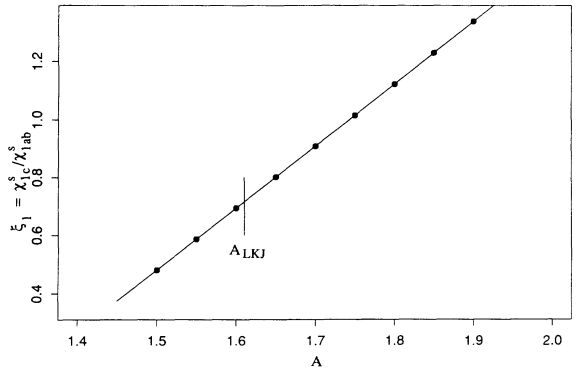

FIG. 9. The anisotropy ξ_1 of the spin paramagnetism at the Cu(1) site derived from the plot of Eq. (7a) (Fig. 8, see text) is plotted as a function of the assumed value A for the room-temperature anisotropy of the total susceptibility. The LKJ experimental value of A is indicated.

With a pure $d_{x^2-y^2}$ ground state having $\lambda/\Delta_{0\,(1)}$ parameters the same as for Cu(2), one would have $\xi_1=0.88$. The admixture effect would increase this, giving under a broad range of conditions $0.88\le\xi_1\le 1$. This rather conservative constraint gives, from Fig. 9, $1.68\le A\le 1.74$. Not unreasonably, then, the analysis confines A to a small range $\sim 6\%$ larger than $A_{\rm LKJ}$. The plots in Fig. 8 are based on a particular choice of the physical parameters discussed above, i.e., the input parameters in Table II and anisotropy $A=1.70$. The corresponding solution parameters are listed in Table III. From the value given for $A^{\rm iso}$ we use the empirical value[8] $A^{\rm cp}\simeq -128$ kG/μ_B to determine the transferred hyperfine constant $B=(A^{\rm iso}-A^{\rm cp})/4$. Using Eq. (9) and the results in Table III we obtain the usual on-site hyperfine parameters to be $A_\perp=-8.7$ kG/μ_B and $A_\parallel=-190$ kG/μ_B.

We return now to the discussion of SFD effects in the K/χ plots of Fig. 8. In the plot based on Eq. (7a) [labeled (ab)], there is a reasonable degree of linear behavior at high temperatures, with a deviation setting in at 125 K and below. This onset seems to be clear evidence for a diamagnetic response which is not reflected in the NMR shift data of Fig. 6. It appears to represent a crossover from 2D fluctuation behavior at high temperatures to 3D behavior in the vicinity of T_c. It is important to note that the input data values for A and $\chi^{\rm dia}$ can be varied in ranges of $\pm 10\%$ without changing the qualitative nature of this result.

The plot of Eq. (7b) [labeled (c)] in Fig. 8 leads to a somewhat more dramatic conclusion, namely that the size and temperature variation of c-axis diamagnetism is such that there is no region below room temperature where the relation $\chi^s_c\simeq\chi^{\rm expt}_c-\chi^{\rm dia}-\chi^{\rm orb}_c$ is asymptotically

TABLE II. Room-temperature shift and bulk susceptibility data used to determine the hyperfine and susceptibility tensors for the individual copper sites. The choice of anisotropy $A=\chi^{\rm tot}_c/\chi^{\rm tot}_{ab}$ is discussed in the text. The shifts are given in percent, the susceptibilities in 10^{-4} emu/mole f.u.

	$K^{\rm orb}_1$	$K^{\rm orb}_2$	K^s_1	K^s_2	$\chi^{\rm expt}$	A
ab	0.675	0.28	0.27	0.293	2.57	1.70
c	0.25	1.28	0.309	−0.01	3.79	

TABLE III. Room-temperature parameter values for Cu-site hyperfine and susceptibility tensors, derived from an iterated solution to Eqs. (1)–(3), (7a), (8), and (9) (see text), using the data values from Table II as input. Units are as follows: α's, (emu/mole)$^{-1}$; χ's, 10^{-6} emu/mole; $\Delta_{0\,(1)}$, eV; $\langle r^{-3}\rangle$, a.u.; $A^{\rm iso}$ and B, kG/μ_B. The value stated for $B=(A^{\rm iso}-A^{\rm cp})/4$ is derived from an assumed value $A^{\rm cp}=-128$ kG/μ_B. These values of χ_ν^s correspond to local anisotropies $\xi_1=0.91$ and $\xi_2=1.28$.

ν	g_ν	α_ν^s	$\chi_\nu^{\rm orb}$	χ_ν^s	Misc. parameters
1*ab*			54.1	95.7	$\Delta_0=2.04$
1*c*		35.6	20.1	86.9	$\Delta_1=2.33$
2*ab*	2.075	30.4	22.5	96.4	$\langle r^{-3}\rangle=5.57$
2*c*	2.345	−0.8	102.6	123.0	$A^{\rm iso}=56.6$
					$B=46.2$

correct. We therefore conclude that a substantial temperature-dependent component $\chi_c^{\rm SFD}(T)$ is present. In order to interpret this result we fit the data to the asymptotic form $\chi_c^{\rm SFD}\propto T^{-1}$ as $T\to\infty$ derived by Nagaosa and Lee[9] (see also the result of Ioffe and Kalmeyer[10]). This form leads us to conclude that $\chi_c^{\rm SFD}(300$ K) [in emu per mole of Cu(2) sites] is roughly -6% of $\chi_{2c}^s(300$ K). Because of this, the straight line labeled (c) in Fig. 8, which represents Eq. (7b) when $\chi_c^{\rm res}=\chi_c^s$, falls somewhat below the data points. With $\chi_c^s(T)$ thus determined, $\chi_c^{\rm SFD}(T)$ then follows from Eq. (1). Values of $\chi_{ab}^{\rm SFD}$ and $\chi_c^{\rm SFD}$ obtained in this fashion are plotted against temperature in the inset to Fig. 8, in units of $2\chi_{2c}^s(300$ K). The scale therefore gives the diamagnetism as a percentage of the room-temperature spin paramagnetism of the planes in the Y-Ba-Cu-O structure.

Because the result for $\chi_c^{\rm SFD}(T)$ is qualitatively different from that of LKJ and is based on virtually the same susceptibility data, it is important to pinpoint the origin of this disparity. A careful examination shows that the difference arises almost entirely from the anisotropy of the spin paramagnetism, which stems in turn from the the anisotropic g factors [Eq. (8)]. Without this, i.e., with ξ_1 and $\xi_2=1$, the deviation of the data from the behavior of Eq. (7b) is much smaller.

IV. DISCUSSION AND CONCLUSIONS

This study has endeavored to accomplish three goals: first, to use precise measurements of the normal-state NMR shifts and susceptibilities of Y-Ba-Cu-O to effect a partition of the spin susceptibilities between the Cu(1) and Cu(2) sites; second, to derive at the same time a complete characterization of the susceptibility and (copper) hyperfine tensors of the material; finally, by comparing the total behavior of spin and orbital susceptibilities determined in this process with experimental measurements, to note the presence of an additional temperature-dependent "anomalous" diamagnetism.

The intrinsic susceptibility of the Y-Ba-Cu-O sample employed in this work, as reflected in the behavior of paramagnetic NMR shifts, is argued in Sec. II to be equivalent to that of any high-quality, well-oxygenated material, and in particular to that of the LKJ sample. The powder average susceptibility data bear this out in showing the difference between samples to be purely Curie like. Through comparison of oriented-powder data with that of LKJ we find, however, that the Curie effect is distinctly anisotropic. The validity of the Curie anisotropy is supported by the precise match (better than 0.5%) in scale factors S (Table I) for the intrinsic terms. In the absence of any compelling reason to question the basic correctness of this result, we propose to accept it as an experimental fact. It could, for example, easily stem from Cu^{2+} sites in the lattice which have become localized through disorder. It is interesting to note that the anisotropy found for C matches within experimental error that of $\chi_{2\nu}^s$ given in Table III.

It follows from the fits to Eq. (5) (Fig. 2 and Table I) that the changes in our own data from grinding and epoxification are also Curie like. On this basis we could correct our raw data without reference to that of LKJ to achieve straight-line behavior with Eq. (7a) in Fig. 8. The resulting isotropic Curie corrections would lead to a similar result for $\chi_c^{\rm SFD}$ as that found, with perhaps a slightly smaller amplitude. On the other hand, this procedure leads to a discrepancy between our intrinsic susceptibilities and those of LKJ, for which we believe there is no physical basis.

The current data and analysis demonstrate the existence of the temperature-varying diamagnetism $\chi_c^{\rm SFD}(T)$ shown in Fig. 8 (inset), but probably do not determine its magnitude with high accuracy. In the first place, it is very small compared with the other terms, and, moreover, it has the same temperature dependence as the spurious term. It is, however, 100% anisotropic well above T_c, and can be distinguished on that basis. The presence of a background Curie term beyond the susceptibility corrections applied in Sec. II can, in principle, be detected through the data plot according to Eq. (7a), where it would produce a downward curvature. Whether such an effect is present in Fig. 8 is not well resolved. It should be emphasized that the diamagnetism anomaly we find is strongly dependent on the anisotropy of the spin paramagnetism, i.e., of the g factors [Eq. (8)]. Given the extraordinary success of the ionic model employed by MR to describe the magnitude and anisotropy of both the spin and orbital NMR shifts, as well as the anisotropy of T_1, there is ample reason to suppose that the g-factor anisotropy dictated by the ionic model is also present. For example, the basic ingredients of spin-orbit coupling and crystal-field splitting give rise to similar g-factor effects in fcc Cu metal.[37] Their absence here would not only run contrary to known behavior in other systems, but would also require the susceptibility anisotropy A to be ~ 1.50, in contradiction to the higher measured value

$A_{LKJ}=1.61$.

The plot of Eq. (7a) is also a crucial step in our deduction of susceptibility and hyperfine parameters (Table III) and, in particular, the partition of χ_v^s between the chains and planes. The latter breakdown consists of roughly equal contributions from Cu(1) and Cu(2) sites, consistent with the assumption of MR. We also note that the parameter determination presented here (Table III) not only partitions $\chi_v^s(T)$, but also takes account of the anisotropy of the constituents and derives all parameters from static magnetic and hyperfine data on this system. With the deduction scheme employed in Sec. III, a satisfactory result is only obtained if the anisotropy A (Fig. 9) is slightly larger than the value $A_{LKJ}=1.61$, which is a very reasonable outcome.

It is useful to mention some comparisons between the parameters in Table III and data from the literature. The value we obtain for $\langle r^{-3}\rangle$ (5.57 a.u.) is somewhat smaller than the Cu^{2+} impurity value (6.3 a.u.) employed by MR.[8,15] This is not unreasonable, since the metallic oxides are more strongly covalent than the salts from which the ionic value is derived.[15] On the other hand, our value is substantially larger than those (<5 a.u.) deduced for broad-band $3d$ metals,[32] which also seems appropriate. Theoretical estimates of the crystal-field splittings Δ_0 and Δ_1 by McMahon, Martin, and Satpathy[33] agree within a few percent of the values obtained. In addition, we may use the hyperfine parameters obtained [Eq. (9), Table III] to estimate the spin-lattice relaxation anisotropy[34] for the Cu(2) sites. Neglecting spin-spin correlations, we find $T_{1ab}/T_{1c}\approx 2.9$ at room temperature. Since correlations will tend to increase this ratio,[34] the foregoing value is at least consistent with experimental data[35,36] giving $T_{1ab}/T_{1c}\approx 3.6$.

Regarding the $\chi_v^{SFD}(T)$ results (inset, Fig. 8), the observed behavior gives important insights into the normal-state properties of this system. The onset of χ_{ab}^{SFD} at $\approx T_c+35$ K shows that the high-temperature fluctuations are two dimensional in character, but that the superconducting transition is 3D, as has been noted elsewhere.[2] The c axis result shows that temperature-dependent fluctuation diamagnetism extends to and quite possibly beyond room temperature. These data are seen in Fig. 8 to be consistent with the asymptotic form $\chi_c^{SFD}(T)\propto T^{-1}$ predicted by Nagaosa and Lee, [9] and are similar to the predictions of Ioffe and Kalmeyer as well.[10] Finally it is well to mention other work related to the question of the existence of chiral gauge fluctuations in these systems. Recent theoretical work by Shastry and Shraiman[38] points up the fact that such fluctuations give rise to Raman scattering effects with special symmetries, by which their presence could be convincingly established. Perhaps the present work may stimulate further studies along those lines.

ACKNOWLEDGMENTS

The authors wish to thank N. Nagaosa and P. A. Lee and also L. Ioffe and V. Kalmeyer for communication of their respective results before publication and for discussions. We also thank A. Millis, P. Littlewood, and S. Shastry for many informative discussions.

APPENDIX

In this appendix we derive certain relations concerning the magnetic response of a specimen consisting of a large number of partially oriented crystallites. Each crystallite is assumed to have a susceptibility tensor given by

$$\vec{\chi}=(\hat{\mathbf{i}}\hat{\mathbf{i}}+\hat{\mathbf{j}}\hat{\mathbf{j}})\chi_{ab}+\hat{\mathbf{k}}\hat{\mathbf{k}}\chi_c \ . \tag{A1}$$

We define a set of Cartesian axes, with respect to which the field $\mathbf{H}$ has polar angles Θ and ϕ and the c axis of crystallite i is denoted by Θ_i and ϕ_i. A unit vector in the latter direction is thus given by

$$\hat{\mathbf{c}}_i=\hat{\mathbf{i}}\sin\Theta_i\cos\phi_i+\hat{\mathbf{j}}\sin\Theta_i\sin\phi_i+\hat{\mathbf{k}}\cos\Theta_i \ ,$$

$\hat{\mathbf{i}}$, $\hat{\mathbf{j}}$, and $\hat{\mathbf{k}}$ being the usual Cartesian unit vectors. The angle between $\hat{\mathbf{c}}_i$ and $\mathbf{H}$ is further defined to be Ω_i. The magnetization of the ith crystallite may then be written

$$\mathbf{m}_i=(H\cos\Omega_i)\chi_c\hat{\mathbf{c}}_i+(\mathbf{H}-\hat{\mathbf{c}}_i H\cos\Omega_i)\chi_{ab} \ , \tag{A2}$$

where

$$\cos\Omega_i=\cos\Theta\cos\Theta_i+\sin\Theta\sin\Theta_i\cos(\phi-\phi_i) \ .$$

Equation (A2) may now be summed over i to give the total specimen magnetization. We specify the polar axis to be that direction in space where the average $\langle\cos^2\Theta_i\rangle$ is a maximum, and assume that the specimen has cylindrical symmetry with respect to that axis. Thus, averages such as $\langle\cos\phi_i\rangle$, $\langle\sin\phi_i\rangle$, or $\langle\cos\phi_i\sin\phi_i\rangle$ are assumed to vanish. This is our only assumption regarding the nature of the particle orientations. Carrying out the summation of Eq. (A2), the total magnetization is found to have the form $\mathbf{M}=N_0[\chi_c^{av}\mathbf{H}_c+\chi_{ab}^{av}\mathbf{H}_{ab}]$, where the c axis in this notation is now the polar axis of the specimen. $\mathbf{H}_c$ and $\mathbf{H}_{ab}$ are components of $\mathbf{H}$ parallel and perpendicular to that direction, respectively. The corresponding susceptibility tensor components are

$$\chi_c^{av}=\chi_c\langle\cos^2\Theta_i\rangle+(1-\langle\cos^2\Theta_i\rangle)\chi_{ab} \ , \tag{A3a}$$

$$\chi_{ab}^{av}=\tfrac{1}{2}\chi_c(1-\langle\cos^2\Theta_i\rangle)+\tfrac{1}{2}\chi_{ab}(1+\langle\cos^2\Theta_i\rangle) \ . \tag{A3b}$$

For perfect alignment Eqs. (A3) reduce to the values for a single crystallite. For random orientations ($\langle\cos^2\Theta_i\rangle\rightarrow\frac{1}{3}$), the average tensor components both approach the value $(\chi_c+2\chi_{ab})/3$ as they must.

The controlling parameter in Eqs. (3A) is the polarization $p\equiv\langle\cos^2\Theta_i\rangle$, where $0\le p\le 1$. It is clearly possible to express χ_{ab} and χ_c in terms of the measured tensor components and p:

$$\chi_c=\frac{\chi_c^{av}(1+p)-2\chi_{ab}^{av}(1-p)}{3p-1} \ , \tag{A4a}$$

$$\chi_{ab}=\frac{-\chi_c^{av}(1-p)+2\chi_{ab}^{av}p}{3p-1} \ . \tag{A4b}$$

The value of p may be evaluated at a convenient tempera-

ture and expressed in terms of the measured anisotropy $A_m = \chi_c^{av}/\chi_{ab}^{av}$ and the actual (unknown) anisotropy $A = \chi_c/\chi_{ab}$. Taking the ratio of Eqs. (A3a) and (A3b), we obtain

$$p = \frac{A_m(A+1)-2}{(A-1)(A_m+2)} . \quad \text{(A5)}$$

By substituting this expression into Eqs. (A4), we obtain

$$\chi_c = \frac{\chi_c^{av}[A(A_m+1)-2]-2\chi_{ab}^{av}(A-A_m)}{(A_m-1)(A+2)} , \quad \text{(A6a)}$$

$$\chi_{ab} = \frac{-\chi_c^{av}(A-A_m)+\chi_{ab}^{av}(AA_m+A_m-2)}{(A_m-1)(A+2)} . \quad \text{(A6b)}$$

These equations give the actual susceptibility tensor of the material which would correspond to anisotropy A in terms of the measured anisotropy A_m and the measured tensor components. (Note that in the text χ_c and χ_{ab} are referred to as χ_c^{tot} and χ_{ab}^{tot}, respectively). The susceptibilities can refer to any desired temperature, with the obvious condition that A and A_m must both refer to a single reference temperature. In the text A and A_m refer to room temperature. For a perfectly ordered sample, $A_m \to A$, and χ_c and χ_{ab} in Eq. (A6) then correspond to χ_c^{av} and χ_{ab}^{av} exactly. For a random sample Eqs. (A6) are not useful, since the numerators and denominators both vanish.

[1]B. Batlogg, in *High Temperature Superconductivity Proceedings,* edited by K. S. Bedell *et al.* (Addison-Wesley, Redwood City, CA, 1990), p. 37.

[2]S. E. Inderhees *et al.*, Phys. Rev. Lett. **60**, 1178 (1988).

[3]W. C. Lee, R. A. Klemm, and D. C. Johnston, Phys. Rev. Lett. **63**, 1012 (1989).

[4]S. J. Hagen, Z. Z. Wang, and N. P. Ong, Phys. Rev. B **38**, 7137 (1988).

[5]M. A. Howson *et al.*, J. Phys. Condens. Matter **1**, 465 (1989).

[6]W. E. Lawrence and S. Doniach, in *Proceedings of the Twelfth International Conference on Low Temperature Physics, Kyoto, 1970,* edited by E. Kanda (Keigaku, Tokyo, 1971), p. 361.

[7]M. Miljak, G. Collin, A. Hamzic, and V. Zlatic, Europhys. Lett. **9**, 723 (1989); M. Miljak, V. Zlatic, and I. Kos (unpublished).

[8]F. Mila and T. M. Rice, Physia C **157**, 561 (1989).

[9]P. A. Lee and N. Nagaosa, Phys. Rev. B **43**, 1233 (1991).

[10]L. Ioffe and V. Kalmeyer, Phys. Rev. B **44**, 750 (1991).

[11]S. Barrett *et al.*, Phys. Rev. B **41**, 6283 (1990).

[12]B. Batlogg (private communication). This number results from a survey of core diamagnetism in related compounds, based on data given by *Landolt-Börnstein, New Series, Group II: Atomic and Molecular Physics,* edited by K.-H. Hellwege and A. M. Hellwege, Vols. II/2, II/8, and II/10 (Springer, Berlin, 1966).

[13]The magnetic polarization may be considered to reside on the Cu sites, with the smaller contribution from the oxygen sites included implicitly through hybridization effects. The Ba and Y sites are essentially magnetically inert.

[14]R. Kubo and Y. Obata, J. Phys. Soc. Jpn. **11**, 547 (1956); In this formula $\langle r^{-3} \rangle$ is in atomic units and α_{orb} in units of (emu/mole)$^{-1}$.

[15]A. Abragam and B. Bleaney, *Electron Paramagnetic Resonance of Transition Ions* (Oxford University Press, Oxford, 1970).

[16]R. E. Walstedt and W. W. Warren, Jr., Science **248**, 1082 (1990).

[17]R. J. Cava, B. Batlogg, C. H. Chen, E. A. Rietman, S. M. Zahurak, and D. Werder, Phys. Rev. B **36**, 5719 (1987).

[18]W. C. Lee and D. C. Johnston, Phys. Rev. B **41**, 1904 (1990).

[19]H. Alloul, T. Ohno, and P. Mendels, Phys. Rev. Lett. **63**, 1700 (1989).

[20]R. E. Walstedt *et al.*, Phys. Rev. B **38**, 9299 (1988).

[21]A. Junod, A. Bezinge, and J. Muller, Physica C **152**, 50 (1988).

[22]M. Takigawa *et al.*, Phys. Rev. B **39**, 300 (1989).

[23]M. H. Cohen and F. Reif, in *Solid State Physics,* edited by F. Seitz, and D. Turnbull (Academic, New York, 1957), Vol. 5, p. 321.

[24]H. Riesemeier *et al.*, J. Appl. Phys. **26**, Suppl. **26-3**, 2137 (1987).

[25]G. Balakrishnan, R. Dupree, I. Farnan, D. McK. Paul, and M. E. Smith, J. Phys. C **21**, L847 (1988).

[26]R. E. Walstedt, W. W. Warren, Jr., R. F. Bell, R. J. Cava, G. P. Espinosa, L. F. Schneemeyer, and J. V. Waszczak, Phys. Rev. B **41**, 9574 (1990).

[27]The tensor components χ_{1a}^s and χ_{1b}^s are combined here into an averge in-plane value $\chi_{1ab}^s = (\chi_{1a}^s + \chi_{1b}^s)/2$.

[28]We adopt the ionic model orbital susceptibility expressions given in Ref. 8, namely, $\chi_{2ab}^{orb} = 0.81 N_0(2\mu_B^2/\Delta_1)$ and $\chi_{2c}^{orb} = 0.81 N_0(8\mu_B^2/\Delta_0)$, where the leading numerical factors are estimates of orbital reduction effects, N_0 is Avogadro's number, and μ_B is the Bohr magneton.

[29]We adopt the spin Hamiltonian expressions for $A_\nu^{s.o.}$ given in Ref. 15, p. 456: $A_{ab}^{s.o.} = -\gamma_n\gamma_e\hbar^2\langle r^{-3}\rangle(11\lambda/7\Delta_1)$, and $A_c^{s.o.} = -\gamma_n\gamma_e\hbar^2\langle r^{-3}\rangle(6\lambda/7\Delta_1 + 8\lambda/\Delta_0)$. The measured values of $K_{2\nu}^{orb}$ determine the ratios $\langle r^{-3}\rangle/\Delta_{0(1)}$. With $\lambda = -0.088$ eV (see text), one has, using the shift values from Table II, $A_{2ab}^{s.o.} = 20.7$ (kG/μ_B) and $A_{2c}^{s.o.} = 135.7$ (kG/μ_B).

[30]In keeping with our interpretation of the room-temperature c-axis diamagnetism developed toward the end of this section, we have also taken $\chi_c^{SFD}(300\text{ K}) \approx -6\%$ of $\chi_c^{res}(300\text{ K})$ [see Eqs. (7)] in the parameter determination scheme.

[31]C. H. Pennington, D. J. Durand, C. P. Slichter, J. P. Rice, E. D. Bukowski, and D. M. Ginsberg, Phys. Rev. B **39**, 2902 (1989).

[32]R. E. Walstedt, J. H. Wernick, and V. Jaccarino, Phys. Rev. **162**, 301 (1967).

[33]A. K. McMahon, R. M. Martin, and S. Satpathy, Phys. Rev. B **38**, 6650 (1988).

[34]A. J. Millis, H. Monien, and D. Pines, Phys. Rev. B **42**, 167 (1990).

[35]R. E. Walstedt, W. W. Warren, Jr., R. F. Bell, and G. P. Espinosa, Phys. Rev. B **40**, 2572 (1989).

[36]S. E. Barrett *et al.*, Phys. Rev. Lett. **66**, 108 (1991).

[37]D. L. Randles, Proc. R. Soc. London, Ser. A **331**, 85 (1972).

[38]B. Shastry and B. I. Shraiman, Phys. Rev. Lett. **65**, 1068 (1990) (unpublished).